Mohsen Derakhshan
Department of Mechanical Engineering,
Temple University,
Philadelphia, PA 19122
e-mail: mohsen.derakhshan@temple.edu

Mehdi Gilaki
Department of Mechanical Engineering,
Temple University,
Philadelphia, PA 19122
e-mail: mehdi.gilaki@temple.edu

Andrew Stacy
Department of Mechanical Engineering,
Temple University,
Philadelphia, PA 19122
e-mail: andrew.stacy@temple.edu

Elham Sahraei
Department of Mechanical Engineering,
Temple University,
Philadelphia, PA 19122;
Department of Mechanical Engineering,
Massachusetts Institute of Technology,
Cambridge, MA 02139
e-mail: elham.sahraei@temple.edu

Damoon Soudbakhsh[1]
Department of Mechanical Engineering,
Temple University,
Philadelphia, PA 19122;
Department of Mechanical Engineering,
Massachusetts Institute of Technology,
Cambridge, MA 02139
e-mail: damoon.soudbakhsh@temple.edu

Bending Detection of Li-Ion Pouch Cells Using Impedance Spectra

Li-ion batteries are the preferred choice of energy storage in many applications. However, the potential for fire and explosion due to mechanical damage remains a safety concern. Currently, there are no criteria for the extent of the mechanical damage under which the batteries are safe to use. Here, we investigate the effects of bending damage to Li-ion cells on their impedance spectra. After the initial characterization of four Li-ion pouch cells, one of the cells underwent a three-point bending load. We measured the impedance spectra of this cell after each increment of loading. The impedance data of the control group cells were collected at the same intervals as the damaged cell. A distributed equivalent circuit model (dECM) was developed using the data from the electrochemical impedance spectroscopy (EIS) procedure. We observed that several model parameters such as the magnitude of constant phase elements had similar trends in the control cells and the bent cell. However, some model parameters such as resistances in parallel with constant phase elements, and the inductor showed dependency on the extent of the damage. These results suggest the potential for use of such parameters as an indicator of mechanical damage when visual inspection of cells is not possible in a battery pack setup. Future steps include investigation of similar trends for other commercial batteries and chemistries and form factors to verify the applicability of the current findings in a broader context.
[DOI: 10.1115/1.4049527]

Keywords: electrochemical impedance spectroscopy (EIS), Li-ion batteries, distributed equivalent circuit models (ECMs), control applications, energy storage, fault detection and diagnosis

1 Introduction

Lithium-ion batteries are the preferred choice of energy storage in various applications, including electric or hybrid-electric vehicles [1,2]. Li-ion batteries are susceptible to mechanical damages, which may lead to an electrical short, thermal runaway, and possibly explosions or fires [3]. Consequently, the development of methods to reliably characterize the safety of LiBs is crucial. In the literature, there are extensive studies on the state of charge (SoC) and state of health (SoH) [4–7]. The battery management systems typically estimate SoC and SOH of LiBs [8–10]. The state of charge is mainly related to controlling the charge and discharge of the battery considering cell balancing and thermal condition of the cells [11]. State of health mainly involves capacity fade due to battery aging [12,13] and do not specify the safety of LiB after an incident such as mechanical damage. Previous studies have shown that mechanical damages can cause thermal runaway of the batteries [14–16]. Despite these safety concerns, there are very limited studies on the effects of mechanical damage on the safety of LiBs [4]. Experiments and finite element modeling of Li-ion cells under mechanical loading have shown that the internal short of Li-ion cells happens at the same time as the mechanical failure, when the principal strain components of the cells exceed their failure limits [3,17,18,19]. However, they do not study the cell's electrical response before the failure. Currently, there is no reliable battery characterization method to determine the safety of the batteries for future use after sustaining mechanical damage. The current practice in dealing with such cases is to scrap cells after such incidents even if there are no apparent damages [20]. Typically, battery diagnostic systems detect electrical failures such as short circuits and loose connections. However, studies on detecting the mechanical damage of Li-ion batteries has been very limited and is still an open problem.

Here, we aim at quantifying the effects of mechanical damages on the response of Li-ion cells. Specifically, we look at the bending of Li-ion pouch cells to develop criteria for the safety of cells after sustaining such damages. Pouch cells have been used extensively in many electric and hybrid vehicles such as in Nissan Leaf and Chevy Volt [14]. Our approach to this problem is to measure the impedance spectra of the cells, which is called electrochemical impedance spectroscopy (EIS), and use a distributed equivalent circuit model (ECM) to quantify the response of the cells.

The rest of the article is organized as follows: In Sec. 2, we present the experimental setup including the mechanical bending device and the data collection during the experiments. Modeling of the pouch cells based on distributed equivalent circuit elements is discussed in Sec. 3. Experimental results, the computed model parameters, and discussion of the results are provided in Sec. 4. A summary and concluding remarks are given in Sec. 5.

2 Test Setup and Data Collection

We used pouch cells with dimensions 231.78 mm × 163.51 mm × 7.66 mm with a capacity of about 26.3 Ah. The cells were charged and discharged for five cycles at a slow rate of C/10, followed by

[1]Corresponding author.

Manuscript received August 20, 2020; final manuscript received December 7, 2020; published online January 22, 2021. Assoc. Editor: Murat Inalpolat.

measuring their EIS responses after each cycle at 0% state of charge to record their beginning of life performance. The charge and discharge cutoff voltages were 4.1 V and 3 V, respectively. A potentiostat was used to measure electrochemical impedance spectroscopy. EIS is based on applying sinusoidal input in the form of voltage or current to a cell and measuring the output current or voltage. The ratio of voltage to current is called impedance, which is a complex function, with real and imaginary components. The frequency range was 100 mHz to 2000 Hz.

We setup the EIS system using a four-electrode connection mode with two current-carrying leads, one working sense, and one reference lead. Because of their low impedance, EIS measurements of these batteries were very sensitive to connectors, wiring, and other external influences. To minimize the distortions and achieve repeatable measurements, we designed a fixture to connect battery terminals to the EIS instruments [4]. The current-carrying leads were in direct contact with the fixture's copper plates and fastened down with washers and nuts. Each copper plate also had a connection port for the reference and working sense leads, respectively. Also, to secure the cell and create a consistent connection between the electrodes and copper plates, an additional screw was used between the two electrodes. Superconductive copper plates were used for the fixture to ensure very low impedance (0.1 mΩ). The experiments were conducted using an excitation voltage of 10 mV.

The three-point bending test was conducted using an Instron 5985 universal load frame. A fixture was designed and manufactured for this purpose (see Fig. 1(*a*)). The bottom part of the fixture including the supporting rods was connected to the bottom rod of the load frame, and the indentor rod was connected to the moving part of the frame. An linear variable displacement transducer (LVDT) deflection sensor was connected to the fixed and moving parts of the fixture to be able to measure the deflection of the battery accurately. The distance between the two supporting rods was 140 mm, and the diameter of all three rods (supports and indentor) was 15.8 mm. Following initial characterization and charge/discharge cycles, the discharged cell (at 0% SOC) was placed on the supporting rods in the longitudinal direction. The displacement was applied using the indentor at a rate of 1 mm/min. During the mechanical loading, force, crosshead displacement, LVDT displacement, and voltage were measured using the load frame's software. The three-point bending test was stopped intermittently at the displacements of 1, 2, 4, 8, 10, and 12 mm to perform EIS measurements. The duration of each stop was 20 min and a 10-min relaxation time followed by the time needed for EIS measurement.

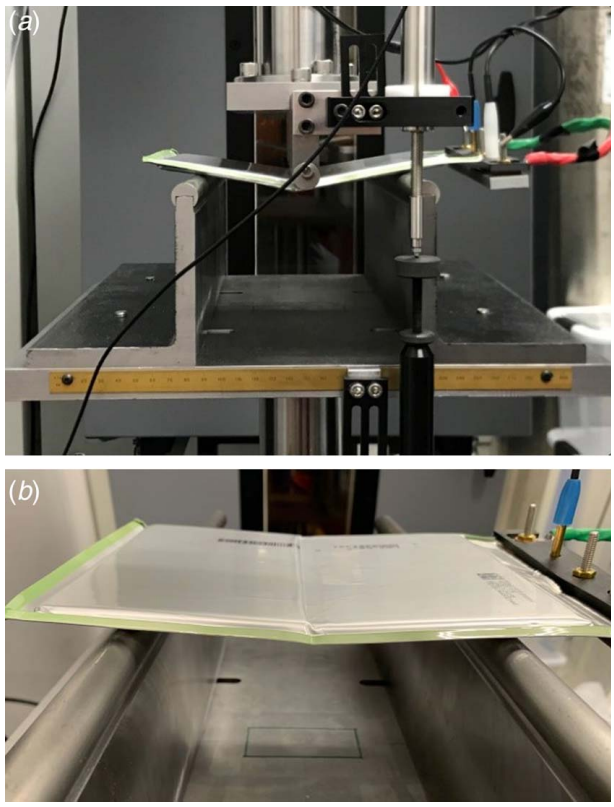

Fig. 1 (*a*) Bending setup and connections for EIS measurements and (*b*) deformation of the battery after bending

3 Modeling

We modeled the cells using a distributed equivalent circuit model as shown in Fig. 2. The model parameters were found using the impedance spectra of current-voltage. The model is an adapted Randles model [21,22] and consists of an inductor, three resistors, and three distributed elements. These elements are related to different aspects of the electrochemical processes of the cell, including conductivity loss, the formation of the solid electrolyte interface, charge transfer, double-layer capacitance, and finite diffusion. For example, starting with Fick's law [21] for the diffusion process and solving for a steady-state solution with reflective boundary condition, one can get to a form similar to the distributed element Z_{BW}, which is called the finite-space Warburg element and can be estimated as follows [21]:

$$Z_{BW}(\omega) = \frac{1}{Y_0\sqrt{j\omega}}\coth B\sqrt{j\omega} \tag{1}$$

where ω is the frequency in rad/s and B and Y_0 are the parameters of the Warburg element, which are calculated in the curve-fitting process. At low frequency, the Warburg element can be simplified to a resistance and a capacitor in series, so by having the Nyquist diagram, the initial guess (or minimum value) of B/Y_0 can be obtained using the following relation [21]:

$$Z_{real}(\omega \to 0) = \frac{B}{3Y_0} \tag{2}$$

The initial guess of Y_0 can be calculated as follows [4]:

$$\frac{1}{Y_0\sqrt{j\omega}} = \frac{RT}{(n_eF)^2C^o\sqrt{j\omega D}} \tag{3}$$

where n_e is the number of electrons transferred per mol of reaction species, F is the Faraday's constant, R is the universal gas constant, T is the temperature in Kelvin, and C is the Li^+ ion concentration. Similarly, the constant phase elements (CPEs) arise from the distributed nature of microscopic material properties on the surface of the electrodes and can be estimated with the following impedance form:

$$Z_{CPE} = \frac{Q}{(j\omega)^n} \tag{4}$$

where n is the condition number of the CPE and Q is a scaling factor. The condition number varies between zero and one, so CPE is simplified to an ideal resistor and ideal capacitors at the boundaries, and $n = 0.5$ represents an infinite Warburg element. Thus, for each CPE element, there are two unknown parameters Q_{CPE} and n_{CPE}, which should be calculated in the curve-fitting process.

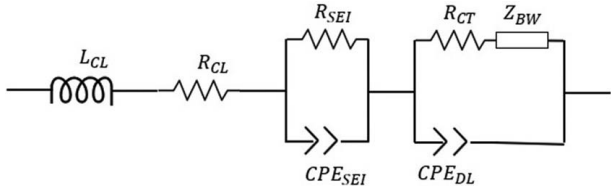

Fig. 2 Distributed equivalent circuit model

Complex nonlinear least squares was used to estimate the model parameters based on the measured impedance spectra (real and imaginary components of the impedance). To avoid unrealistic model parameters, we provide the starting values and constraints based on the nominal measurements of the battery parameters (e.g., see Ref. (3)) and the measured EIS. Sum of the weighted errors (χ^2), residuals, and element errors was used to evaluate the quality of the curve fitting. For an acceptable curve fitting, we require $\chi^2 < 10^{-4}$. The sum of the weighted squares is calculated using the following equation:

$$\chi^2 = \sum_{i=1}^{k} \left(\frac{(Z_{i,R} - Z_{i,RE})^2}{Z_{i,RE}^2} + \frac{(Z_{i,I} - Z_{i,IE})^2}{Z_{i,IE}^2} \right) \tag{5}$$

In Eq. (5), $Z_{i,RE}$ and $Z_{i,IE}$ are the estimated values of the measured real $Z_{i,R}$ and imaginary $Z_{i,I}$ impedance. Kramers–Kronig (K-K) transform was used to validate the measured EIS data with causality, stability, linearity, and fitness of response conditions [4]. There are ten unknown parameters of the system that were obtained using complex nonlinear least squared curve fitting [21].

4 Results

After the initial characterization of the cells as described in Sec. 2, one cell (cell D) was selected to undergo three-point bending and EIS measurements. The EIS measurements were followed by modeling to investigate the effects of cell's deformation due to three-point bending on the model parameters. For the bending experiment, the applied displacement, the measured force, and the start time of each EIS measurement are shown in Fig. 3. The force–displacement curve shows that at a displacement value of about 2.7 mm, and the force reaches a peak of 370 N after which it drops with a smaller slope. The experiment was continued up to 12 mm of displacement without any sign of an electric short circuit in the cell or a significant drop in its voltage (the battery after bending experiment is shown in Fig. 1(*b*)). The starting voltage for the cell that underwent bending was 2.80 V, and it dropped to 2.78 V after the experiment, which corresponds to a drop of about 20 mV. We measured EIS at multiple steps, as shown in Fig. 3. The displacements were held constant during the EIS measurements, which resulted in drops in the measured forces. However, the forces would rise to the pre-EIS levels before significant changes in the displacements were observed. The right axis shows the elapsed time from the beginning of the experiments to the end.

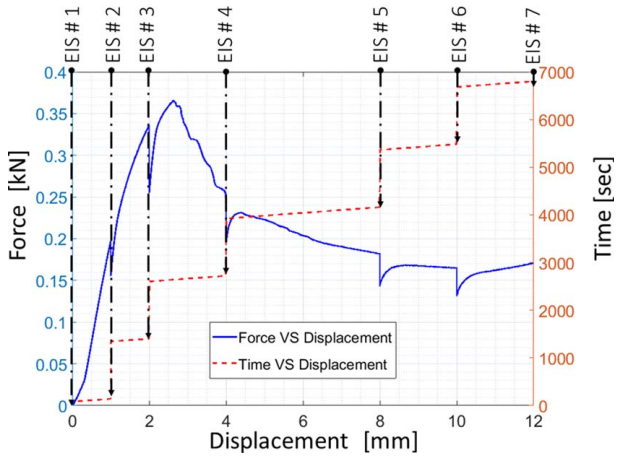

Fig. 3 Force–displacement and the start time of each EIS during cell bending

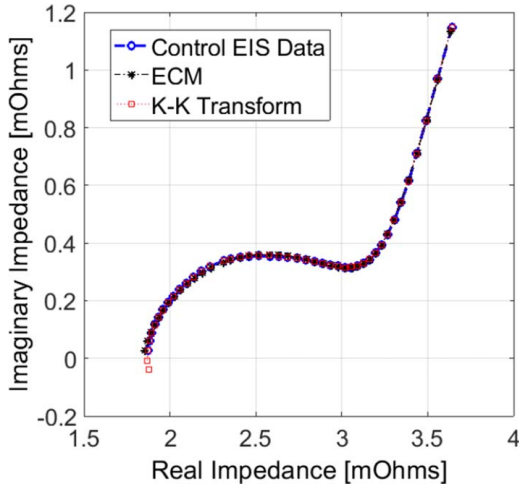

Fig. 4 ECM and K-K transform diagrams for a sample control EIS data

To compare the evolution of EIS measurements between cell D and the control group (cells A, B, and C), we performed EIS measurements in the same temporal space from the initial EIS measurement. The average drop in voltage of the other cells (control group) was about 30 mV. To ensure that the data are valid, we used K-K transforms as described in Sec. 3. ECM parameters were found using a complex nonlinear least square fitting method. Figures 4 and 5 show agreements between the K-K transforms and the measured data for control cells and the bent cell. Figures 4 and 5 show an example of the fitting accuracy for the intact and damaged cell, which shows the accuracy of the model in predicting the frequency response of the cells.

Figure 6 shows R_{CT}, Q_{DL}, and R_{SEI} parameters of the ECM. The vertical axis shows the parameters, and the horizontal axis shows the displacement of cell D. The EIS for the other cells were performed with the exact time intervals as cell D from the onset of the experiments to minimize the differences among the trend of ECM parameters due to the relaxation time of the cells after each EIS measurement. Figure 6(*a*) shows that the control cells have relatively constant charge transfer resistance R_{CT}, whereas R_{CT} of the bent cell shows a sharp increase after measuring EIS at 2 mm mechanical displacement. Figure 6(*b*) shows that Q_{DL} has a similar trend for all four cells. Calculated resistance of the solid–electrolyte interface, R_{SEI}, has a slight decrease in the control cells, whereas the trend is reversed when cell D was

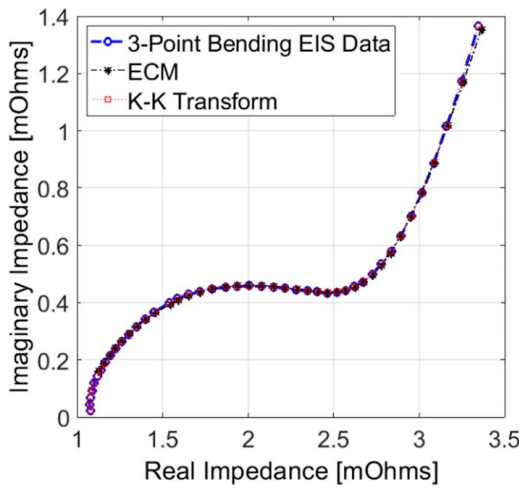

Fig. 5 ECM and K-K transform diagrams for a sample bent cell data

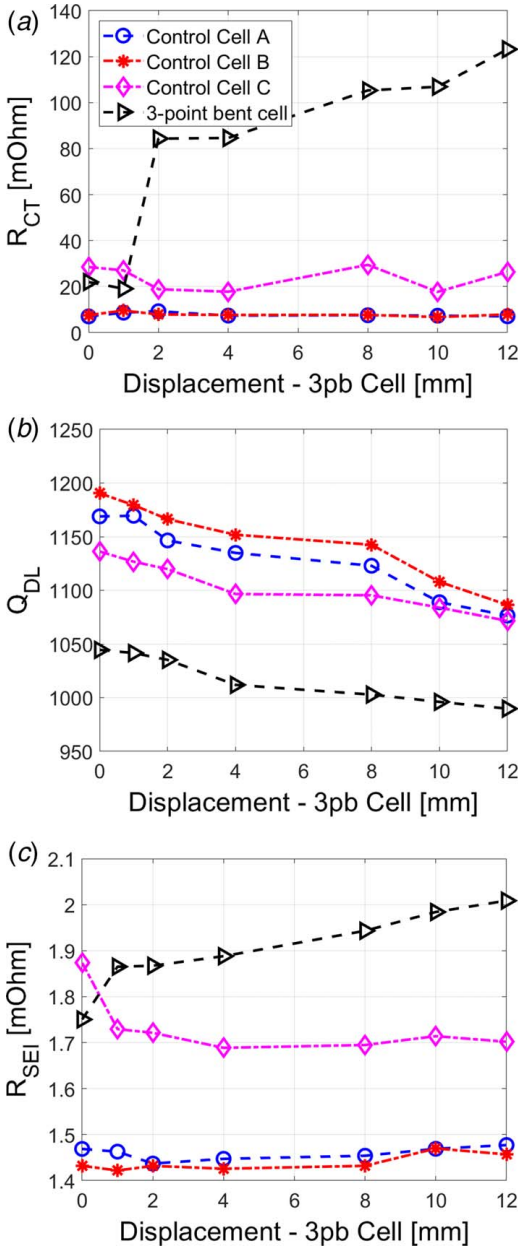

Fig. 6 Trend of model parameters throughout bending and corresponding time for the control samples: (*a*) charge transfer resistance, (*b*) Q of the double-layer CPE, and (*c*) resistance of the SEI layer

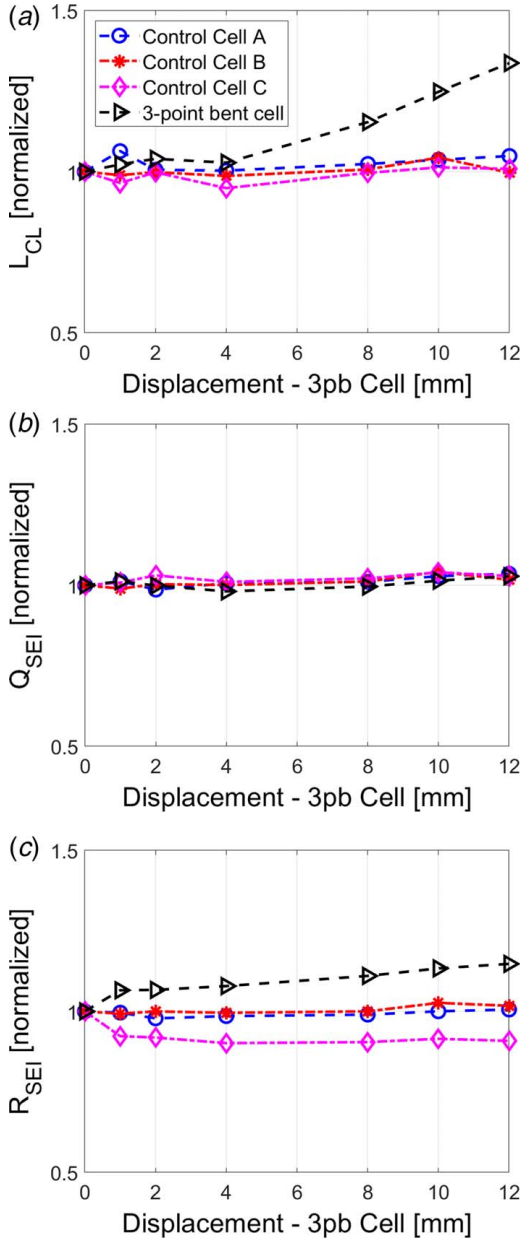

Fig. 7 Trend of normalized model parameters throughout three-point bending and corresponding time for the control samples: (*a*) inductor, (*b*) Q of the SEI layer, and (*c*) resistance of the SEI layer

subjected to the bending experiments, and its value increased with cell bending.

Figure 7 shows the normalized model parameters of the mechanically damaged cell compared to the control group. Here, we show normalized L_{CL}, Q_{SEI}, and R_{SEI} for all cells. The horizontal axis shows the displacement of cell D. The other EIS measurements were performed at the exact time as the EIS measurements of cell D. The time intervals are reported in Fig. 3. The trend of the normalized inductance is shown in Fig. 7(*a*). Figure 7(*b*) shows the normalized values for Q_{SEI}, and this value remained relatively constant for the control groups and the mechanically damaged cell. The control group has a relatively constant inductance for all the EIS measurements, whereas the bent cell shows over 30% increase in this parameter. Figure 7(*c*) shows resistance from the solid electrolyte interface of the cells. Instead of a constant value as in the control cells, R_{SEI} increased by the bending of the cell.

5 Summary and Conclusions

In this study, a Li-ion pouch cell was subjected to an ideal three-point bending scenario and incrementally damaged. During the mechanical loading, the test was intermittently stopped to perform EIS measurements. Three control cells were also used to perform EIS measurements to compare test parameters with the damaged cell. The EIS measurements on the control cells were performed with the same time intervals as the mechanically damaged cell. We used a distributed equivalent circuit model to represent the cells and model their frequency response. We compared the trend of ECM model parameters of the control cells when subjected to multiple EIS measurements to those of the mechanically damaged cell. We observed that some parameters showed the same trend between the two groups, and some of them such as the inductance, resistance of the charge transfer, and resistance due to the solid–electrolyte transfer had a different trend from the control cells. The peak changes in

the parameters happened near the displacement associated with the maximum applied force to the cell, suggesting internal structural damage in the process. The maximum force was about 370 N at a displacement of about 2.7 mm at the center of the cell. While the study suggests a connection between the ECM parameters and the amount of damage to the cells, we should note that for more definitive criteria, more experiments (samples) are required. Also, the test results may differ for another cell with a different material. Future work includes testing more pouch cells and investigating the response of cylindrical cells.

Acknowledgment

This work was supported in part by the Office of Naval Research (Grant No. N000141912351).

Conflict of Interest

There are no conflicts of interest.

References

[1] Tarascon, J.-M., and Armand, M., 2001, "Issues and Challenges Facing Rechargeable Lithium Batteries," Nature, **414**, pp. 359–367.
[2] Sahraei, E., Gilaki, M., Lynch, W., Kirtley, J., and Soudbakhsh, D., 2019, "Cycling Results of Mechanically Damaged Li-Ion Batteries," 2019 IEEE Electric Ship Technologies Symposium (ESTS), Washington, DC, August, pp. 226–230.
[3] Sahraei, E., Campbell, J., and Wierzbicki, T., 2012, "Modeling and Short Circuit Detection of 18650 Li-Ion Cells Under Mechanical Abuse Conditions," J. Power. Sources, **220**, pp. 360–372.
[4] Stacy, A., Gilaki, M., Sahraei, E., and Soudbakhsh, D., 2020, "Investigating the Effects of Mechanical Damage on Electrical Response of Li-Ion Pouch Cells," 2020 American Control Conference, Denver, CO, July, pp. 1715–1720.
[5] Rivera-Barrera, J. P., Muñoz-Galeano, N., and Sarmiento-Maldonado, H. O., 2017, "Soc Estimation for Lithium-Ion Batteries: Review and Future Challenges," Electronics, **6**(4), p. 102.
[6] Sarmah, S. B., Kalita, P., Garg, A., Niu, X.-d., Zhang, X. -W., Peng, X., and Bhattacharjee, D., 2019, "A Review of State of Health Estimation of Energy Storage Systems: Challenges and Possible Solutions for Futuristic Applications of Li-Ion Battery Packs in Electric Vehicles," ASME J. Electrochem. Energy. Convers. Storage., **16**(4), p. 040801.
[7] Tian, H., Qin, P., Li, K., and Zhao, Z., 2020, "A Review of the State of Health for Lithium-Ion Batteries: Research Status and Suggestions," J. Cleaner. Prod., **261**, p. 120813.
[8] Stuart, T., Fang, F., Wang, X., Ashtiani, C., and Pesaran, A., 2002, "A Modular Battery Management System for HEVs," SAE Trans., pp. 777–785.
[9] Verbrugge, M. W., and Conell, R. S., 2002, "Electrochemical and Thermal Characterization of Battery Modules Commensurate With Electric Vehicle Integration," J. Electrochem. Soc., **149**(1), pp. A45–A53.
[10] Schweighofer, B., Raab, K. M., and Brasseur, G., 2003, "Modeling of High Power Automotive Batteries by the Use of an Automated Test System," IEEE Trans. Instrum. Meas., **52**(4), pp. 1087–1091.
[11] Chaturvedi, N. A., Klein, R., Christensen, J., Ahmed, J., and Kojic, A., 2010, "Algorithms for Advanced Battery-Management Systems," IEEE Control Syst. Mag., **30**(3), pp. 49–68.
[12] Chen, L., Lü, Z., Lin, W., Li, J., and Pan, H., 2018, "A New State-of-Health Estimation Method for Lithium-Ion Batteries Through the Intrinsic Relationship Between Ohmic Internal Resistance and Capacity," Measurement, **116**, pp. 586–595.
[13] Andre, D., Meiler, M., Steiner, K., Wimmer, C., Soczka-Guth, T., and Sauer, D., 2011, "Characterization of High-Power Lithium-Ion Batteries by Electrochemical Impedance Spectroscopy. I. Experimental Investigation," J. Power. Sources, **196**(12), pp. 5334–5341.
[14] Smith, B., 2013, "Chevrolet Volt Battery Incident-nhtsa Summary Report," Accid. Reconstr. J., **23**(5), pp. 31–37.
[15] Williard, N., He, W., Hendricks, C., and Pecht, M., 2013, "Lessons Learned From the 787 Dreamliner Issue on Lithium-Ion Battery Reliability," Energies, **6**(9), pp. 4682–4695.
[16] Feng, X., Sun, J., Ouyang, M., Wang, F., He, X., Lu, L., and Peng, H., 2015, "Characterization of Penetration Induced Thermal Runaway Propagation Process Within a Large Format Lithium Ion Battery Module," J. Power. Sources, **275**, pp. 261–273.
[17] Kermani, G., and Sahraei, E., 2017, "Characterization and Modeling of the Mechanical Properties of Lithium-Ion Batteries," Energies, **10**(11), p. 1730.
[18] Sahraei, E., Kahn, M., Meier, J., and Wierzbicki, T., 2015, "Modelling of Cracks Developed in Lithium-Ion Cells Under Mechanical Loading," RSC. Adv., **5**(98), pp. 80369–80380.
[19] Sahraei, E., Bosco, E., Dixon, B., and Lai, B., 2016, "Microscale Failure Mechanisms Leading to Internal Short Circuit in Li-Ion Batteries Under Complex Loading Scenarios," J. Power. Sources, **319**, pp. 56–65.
[20] Mikolajczak, C., Kahn, M., White, K., and Long, R. T., 2012, *Lithium-Ion Batteries Hazard and Use Assessment*, Springer Science & Business Media, New York.
[21] Macdonald, J., and Barsoukov, E., 2005, *Impedance Spectroscopy: Theory, Experiment, and Applications*, John Wiley & Sons, Inc., Hoboken, NJ.
[22] Pastor-Fernández, C., Uddin, K., Chouchelamane, G. H., Widanage, W. D., and Marco, J., 2017, "A Comparison Between Electrochemical Impedance Spectroscopy and Incremental Capacity-Differential Voltage as Li-Ion Diagnostic Techniques to Identify and Quantify the Effects of Degradation Modes Within Battery Management Systems," J. Power. Sources, **360**, pp. 301–318.